Synthesis of Silica-Carbon Particles in a Turbulent H_2-Air Flame Aerosol Reactor

Hendrik K. Kammler, Roger Mueller, Omri Senn, and Sotiris E. Pratsinis
ETH Zurich, Institute of Process Engineering, CH-8092 Zurich, Switzerland

Synthesis of flame-made nanostructured powders was studied, for the first time, at high production rates (up to 700 g/h) in a turbulent diffusion flame reactor, addressing also the required safety concerns. A commercial hydrogen-air burner was used for synthesis of pure silica and composite silica-carbon particles by oxidation of hexamethyldisiloxane. The product powder was collected continuously in a baghouse filter unit and cleaned periodically by air-pressure shocks. The effect of the fuel (hydrogen) flow rate, powder production rate and total oxidant flow rate on product particle size, morphology, and composition was also investigated. Nitrogen adsorption, transmission electron microscopy and thermogravimetric analysis coupled with a mass spectrometer, and a CO_2-analyzer were employed to characterize specific surface area and powder composition. Typically, aggregates of silica-carbon composite particles (0 to 1.4 wt. % carbon) were made on specific surface areas of 75 to 250 m^2/g at production rates of 125 to 700 g/h, which correspond to particle concentrations of 17 to 93 g/m^3 (2–10% solid fraction by weight).

Introduction

Flame aerosol technology is used for large-scale manufacture of pigmentary titania, carbon black, fumed silica and alumina, lightguide performs, and nuclear fuel pellets to name a few (Ulrich, 1984). Research in this field was motivated from the commercial importance of carbon black since the 19th century, and for fumed silica that was first marketed by Degussa under the name Aerosil, since the mid-20th century (Kloepfer, 1942). Properties like UV protection, electrical conductance, range of darkness, opacity and reinforcement can be achieved, when adding carbon black to elastomers, plastics and paints (Donnet et al., 1993). Silica is used to control thickening, thixotropy, reinforcement, and free flow of liquids and solids, and is utilized to stabilize suspensions, as well as agent for chemical mechanical polishing (CMP) during integrated circuit (IC) fabrication (Sniegowski and de Boer, 2000). Recent reviews have been written for the flame manufacture of silica particles (Pratsinis, 1998) and carbon black (Donnet et al., 1993).

Recently, carbon-silica particles to be used as dual phase fillers have been developed by Cabot Corporation treating carbon black with silica (Francis et al., 1996), opening a new generation of reinforcing agents for rubber (Wang et al., 1998). The combination of carbon black and silica is more effective in reinforcing rubber as compared to carbon black alone providing the capability for the manufacture of so-called "green tires." As the silica surface is covered with silanol groups, adding an organosilane coupling agent such as triethoxysilylpropyltetrasulfane (tradename Si-69) forms a silica network in the rubber. This filler-to-filler network enhances the tire reinforcement decreasing the rolling resistance by up to 24%, while wet traction and treadwear are similar to conventional tires (Byers and McNeish, 1997). The carbon is needed to ensure good dispersibility and static electricity dissipation (Bomal et al., 1993; Byers and McNeish, 1997; Donnet et al., 1993). Reducing the rolling resistance of car and truck tires can significantly decrease fuel consumption by 3–5% and 6–8%, respectively (Padula, 1995), and therefore reduce pollution of air and the environment. The specific surface area of silica powders for rubber reinforcement in green tires should be lower than 180 m^2/g (Blume, 2000). Carbon coated silica is also used as a precursor powder in silicon carbide production (Koc and Cattamanchi, 1998) or for opaque silica aerogels (Lee et al., 1995).

Clearly, there is considerable interest in understanding flame synthesis of silica-carbon nanostructured particles in

Correspondence concerning this article should be addressed to S. E. Pratsinis.
Current address of O. Senn: Sulzer-Burckhardt Engineering Works Ltd., CH-8400 Winterthur, Switzerland.

one step and at high production rates. The study of turbulent flames is of considerable importance in connection with most practical burner systems (Glassman, 1996), as almost all industrial combustion takes place in turbulent flow (Bray, 1998). Intense turbulence may effectively increase flame propagation velocities (Glassman, 1996).

Spicer et al. (1998) synthesized up to 15 g/h SiO_2-C powders with carbon contents up to 30 wt. % in a premixed flame using $SiCl_4$ and acetylene as precursor and fuel. A significant increase in the carbon black yield (of up to three times) was detected in the presence of silica compared with a pure acetylene flame of the same equivalence ratio. The enhanced carbon formation was attributed to the presence of silica particles acting as seed nuclei for carbon surface growth, as well as to the chlorine presence reducing the flame temperature. Silica-carbon particles with carbon contents up to 5 wt. % were synthesized in a ring shaped double diffusion HMDSO-oxygen flame at production rates up to 130 g/h by Kammler and Pratsinis (1999). Briesen et al. (1998a) reported soot formation (up to 2 wt. %) when producing 30 g/h of powder in an electrically assisted flame using ring electrodes. Similarly, Kammler and Pratsinis (2000) found that soot appeared in the product powder when an external electric field was applied by needle and plate electrodes. The soot concentration increased (up to 1 wt. %) with increasing electric field intensity.

The objective of this study is to investigate continuous, high production rate (up to 700 g/h) of silica and silica-carbon particles with controlled composition in a pilot-scale, turbulent air-hydrogen diffusion flame aerosol reactor, using baghouse filters. However, producing large amounts of product powder in a hydrogen-air reactor requires a thoroughly planned safety concept, including active and passive hydrogen safety precautions and ability for a fast shutdown of the pilot plant. Employing hydrogen as fuel and HMDSO as precursor allowed simultaneous formation of silica and carbon particles, as both are introduced by HMDSO. The influence of HMDSO concentration, the oxidant (air), and fuel (hydrogen) flow rate on product powder specific surface area, morphology, and composition were studied.

Experimental Studies

Apparatus

Figure 1 shows the experimental setup. The silica precursor hexamethyldisiloxane (HMDSO, Fluka Chemie AG, 99%) is delivered by bubbling clean dry nitrogen gas (PanGas, CH, > 99.999%) through a fritted cylinder, placed into a 2 L Woulffian flask (Duran) filled up to 3/4 with HMDSO. Fresh HMDSO was supplied continuously into that flask by a gear pump (Gather) from a second flask (10 L) in order to main-

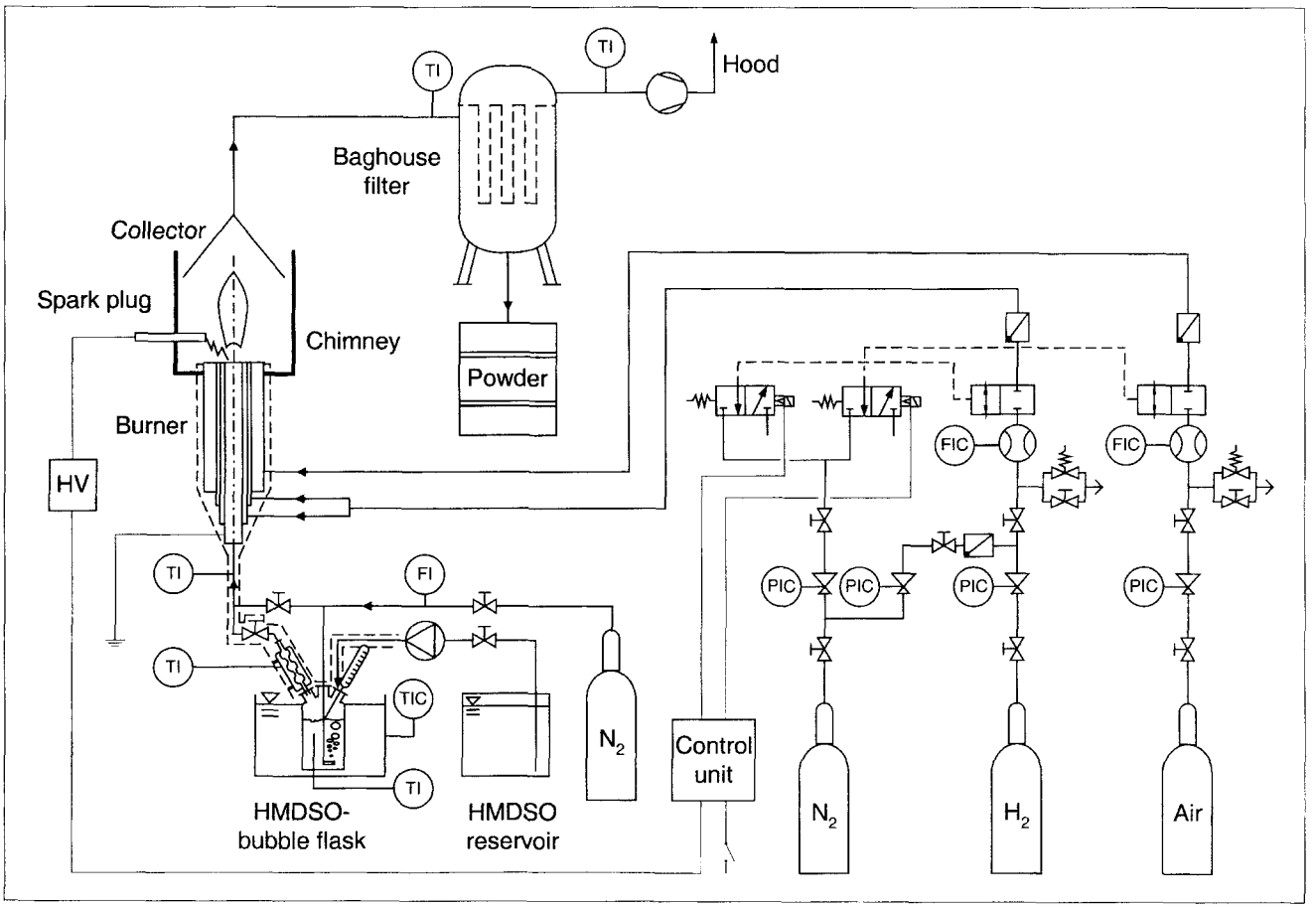

Figure 1. Experimental setup for the continuous production of silica and silica-carbon nanoparticles from HMDSO in a hydrogen-air flame.

tain a constant, level of liquid HMDSO to keep the saturation of the carrier gas constant, even at the highest production rates (Kammler and Pratsinis, 2000). The Woulffian flask is stored in a thermostated bath (Huber Kältemaschinenbau GmbH) to assure a stable HMDSO temperature and delivery during the experiment. The gases are metered by calibrated mass-flow controllers (Hastings Inc., HFC 203) and rotameters (Vögtlin Instruments AG). Between the burner and the HMDSO flask, a 30 cm long Pyrex Allihn-condenser is installed. The cooling chamber of the condenser is filled with water, which is heated by a heating tape and the exit is filled with glass wool in order to prevent entrainment of small HMDSO droplets into the burner (Kammler and Pratsinis, 1999). The tubing between the flask and the burner is heated at least 40 K higher than the HMDSO flask.

A stainless steel hydrogen-air diffusion burner (Deutsche Forschungsanstalt für Luft- und Raumfahrt e.V.), which is typically used as a preheating unit in a downflow reactor (Geier, 1998) was modified by adding two more concentric tubes for gas delivery. The burner then consists of four concentric stainless steel tubes of 0.5 mm wall thickness each. The diameter of the center (first) tube is 6 mm, while the spacing between the following three tubes is 1, 0.5 and 3.5 mm. The outer air (PanGas, CH, synthetic grade) delivering tube (tube 4) had to be designed larger than the other tubes not to create supersonic velocities in the burner, as it was planned to provide an excess of air for combustion. The HMDSO-laden nitrogen stream is fed through the first (center) tube while hydrogen (PanGas, CH, $> 99.5\%$) is supplied through the second and third tubes, thus preventing particle deposition on the burner. The flow rate of nitrogen was 10 L/min, for hydrogen, 12.2 to 42.5 L/min and for air, 69 to 171 L/min (at 25°C and 1.013 bar). The corresponding Reynolds numbers based on the overall nozzle diameter $D =$ 19 mm (Tacke et al., 1996) $Re_D = u \cdot D/\upsilon$ are in the range of 3,000 to 16,000, where u and υ are the velocity and the kinematic viscosity of the reactant stream. The flame is ignited with a spark plug, which is withdrawn after ignition. The flame is encased in a top-open 350 mm diameter steel chimney (Figure 1) to shield the flame over its entire length and to prevent air entrainment from the surroundings. A Plexiglas window allows visible monitoring of the combustion process.

The particle collection unit consists of a commercial Jet filter (Friedli AG, FRR 4/1,6), with four PTFE (polytetrafluoroethylene, Teflon) coated Nomex baghouse filters (total surface area: 2.2 m^2) for powder collection. The filters are set in a stainless steel filter house (2.5 m high and 0.6 m in diameter), which has an inlet 0.6 m long, and a 0.12 m diameter pipe with a cone at its open end over the burner (Figure 1). The particles are collected on the outside of the baghouse filters by an air suction ventilator (Stäfa, 0.75 kW, 50 Hz) controlled by a frequency transducer (Danfoss, AG, VLT 6000 HVAC). The particles are ejected every 70 s from the baghouse filters by air pressure shocks (timing pulse: 30–300 ms) using 5 bar absolute pressure. The product particles are collected in a removable container at the lower part of the filter house.

Safety

Between the mass-flow controllers and the burner, pneumatic ball valves (Bachofen AG) are installed (Figure 1). These nitrogen-pressured ball valves open when another electro-pneumatic ball valve opens the nitrogen reservoir. These valves are closed when either the energy supply or pressured nitrogen lines (operating the ball valves) are interrupted (Geier, 1998). Additional check valves are installed right before the gases enter the burner to avoid backflow of the gases. The whole piping was designed to withstand explosions (Geier, 1998). The gas-pressure reduction of air and hydrogen is made in two stages (Figure 1): from 200 bar (gas cylinder) to 25 bar, and from 25 to 8 bar, which is close to the optimal operating pressure for the mass-flow controllers (6.5 bar), as the gas pressure is crucial for maintaining constant mass-flow rates. The electronic control unit permits remote valve control, ignition with the spark plug, and fast shutdown in case of operational problems. If one of the valves exceeds the pre-set range for reliable operation, the control automatically shuts down the flame reactor. The hydrogen and air supply lines delivering the gas from the cylinders to the flow controllers are fitted with mechanical safety valves that are connected to the vent. The opening pressure is adjusted to 25 bar. As the mass-flow controllers can withstand up to 30 bar, they would not get damaged even in the unlikely case that both mechanical pressure controls would fail because the system pressure would never exceed 25 bar. For flame ignition, the hydrogen control was opened in a so-called slow mode, therefore without overshooting after the constant air flow was already established and the spark plug was on. As an additional passive safety feature, the laboratory is equipped with hydrogen sensors that activate ventilation, and the release alarm and aeration of the laboratory, at 40% of the lower explosion limit of hydrogen in air mixtures (Geier, 1998).

Characterization

The HMDSO-concentration is calculated from the measured supplied volume of HMDSO to the burner at a constant carrier gas-flow rate. The flask temperature is measured by a calibrated K-Type thermocouple (Thermoax), as well as the outside wall temperature of the heated manifold and the filter inlet and outlet gas stream. They are monitored on a personal computer using LabVIEW software. The HMDSO saturation in the nitrogen stream is calculated by a mass balance for the precursor flask, using the HMDSO equilibrium vapor pressure (Boublik et al., 1984). The flame location and height are determined visually. Here, the length of the flame is defined as the distance between the burner mouth and the end of the luminous zone. The reactant flow in the flame is characterized by the air-number, λ, which is defined as the relative value of the effective (actual) amount of fuel (hydrogen and HMDSO) to oxidant to the stoichiometric amount of fuel to oxidant. The air-number is most useful for premixed flames and is the inverse of the equivalence ratio ϕ (Turns, 1996).

The specific surface area A_S of the powder is determined from a five point nitrogen adsorption isotherm in the relative pressure range of 0.05 to 0.25 at 77.3 K (BET analysis) with a Gemini III 2375 (Micromeritics Instruments Corp.). Before the adsorption, the samples are degassed (Flow prep 060, Micromeritics Instruments Corp.) under nitrogen atmosphere at 150°C for 2 h, to remove water that is bound to the particle surface from the air moisture. Nonporous particles are made as shown for selected powders with full isotherm analysis with

an ASAP 2010 (Micromeritics Instruments Corp.). The BET-equivalent average primary particle diameter of the powder can be calculated by $d_p = 6/(\rho_p \cdot A_S)$, where ρ_p is the density of SiO_2, 2.2 g/cm^3.

All experiments are reproduced at least twice on different days and the specific surface area of the product powder from each experiment is measured, at least, twice. Data points are averages of these results, while the error bars in all figures show two times the corresponding standard deviation.

The carbon fraction of the collected powders is determined by thermogravimetric analysis (TGA) in a thermobalance (TGA/SDTA851^e, LF/1100°C, Mettler Toledo AG). The powders are heated up from 25 to 120°C using a heating rate of 10°C per min, held at this temperature for 10 min (first step), then heated up with 20°C per min to 800°C, and held at this temperature for 10 min under nitrogen (PanGas, CH, > 99.999%) atmosphere (second step). Then, the atmosphere is switched to oxygen (PanGas, CH, > 99.95%) and the sample is heated with a heating rate of 20°C per min to 1,000°C and held at this temperature for 5 min. The carbon fraction is attributed to the loss in weight from 800 to 1,000°C (third step). The isothermal segments were inserted to assure that the examined reaction (step) is completed. Each thermogravimetric analysis was performed at least twice on each powder. During the thermogravimetric analysis, a quadrupole mass spectrometer (Quadstar 422, Balzers Instruments) is connected to the thermobalance to detect volatile compounds from the powders in the effluent gas. The gas composition was monitored continuously always scanning from 1 to 170 Daltons. Nitrogen analysis gas and surrounding atmosphere were analyzed to test the sensitivity of the mass spectrometer (detection limit 2 ppm for CO_2) before silica powders were analyzed. Additionally, the CO_2 concentration of the TGA effluent gas was directly monitored with a CO_2 analyzer (aq-5000, Metersonics, Inc.) that was calibrated with known gas mixtures of nitrogen and carbon dioxide (< 1 and 1,950 ppm CO_2).

Flame temperature measurements were carried out with Pt/13%Rh-Pt thermocouples (R-type, Moser AG). Measuring the flame temperature in a particle-laden flame with a thermocouple at these HMDSO concentrations leads to considerable deposition on the tip of the thermocouples that were cleaned after each measurement. The flame temperatures are corrected for radiation loss according to Collis and Williams (1959). Nevertheless, it should be noted that these measurements are rather qualitative.

Transmission electron microscopy (TEM) pictures were prepared by dipping the carbon coated TEM grids (Ted Pella Inc., Carbon type B on 200 Mesh) into the powder, which was collected onto the baghouse filters. The TEM analysis was performed on a Hitachi H 600 electron microscope operated at 100 kV, using magnifications between 10 K and 30 K.

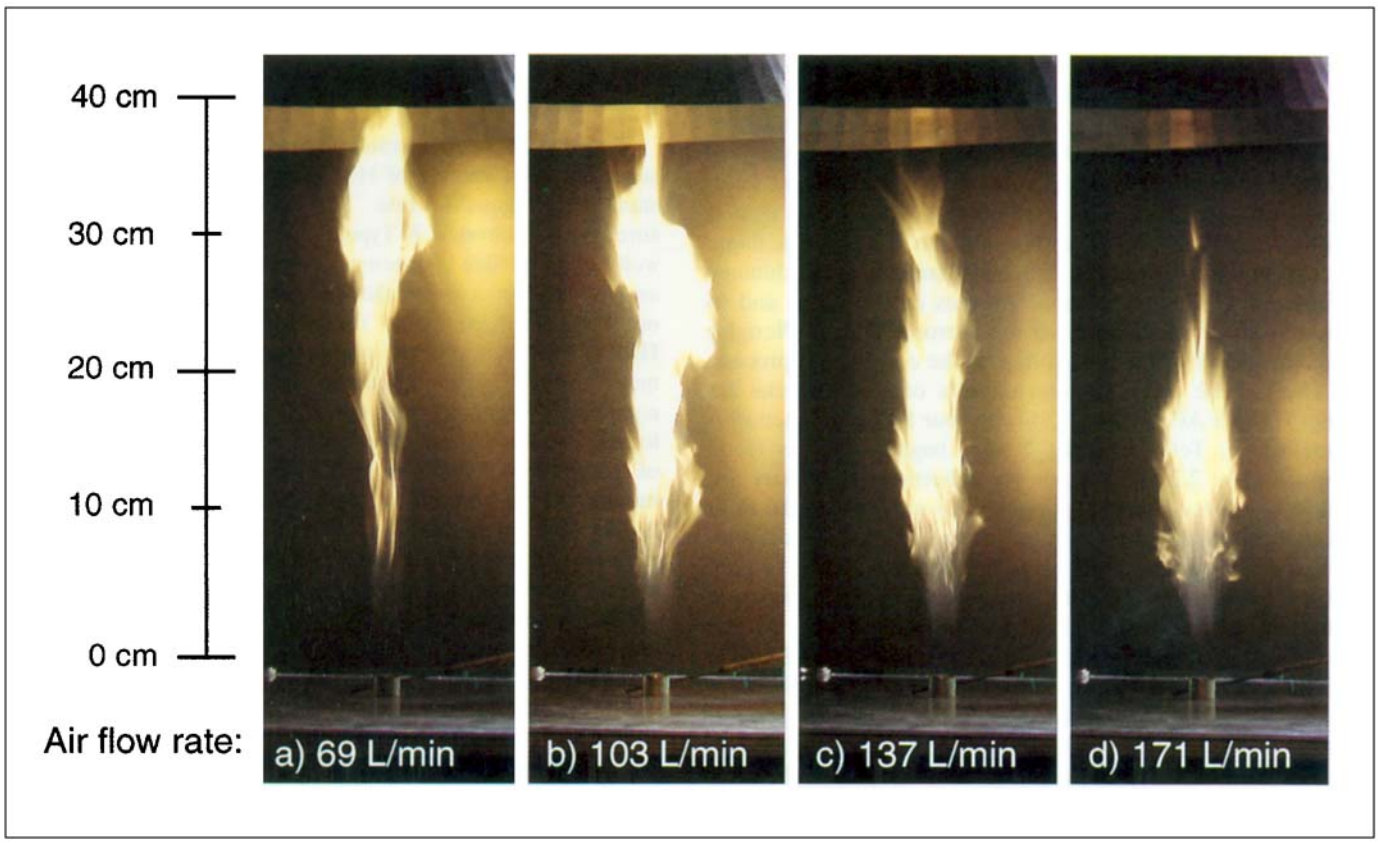

Figure 2. Turbulent diffusion flames for particle production rates of 300 g/h at hydrogen flow rate of 24.3 L/min and at air-flow rates of (a) 69, (b) 103, (c) 137, and (d) 171 L/min.

Analysis of the particles on the micrographs was performed manually counting at least 100 particles. In some cases, particles were analyzed in a JEOL 2010F Scanning Transmission Electron Microscope (STEM) using Energy Dispersive X-ray (EDX) analysis to determine elemental composition.

Results and Discussion

The pure hydrogen flame is about 15 cm long, light blue and almost transparent. This barely visible flame turns into a bright white-yellow flame (up to 70 cm long), when adding HMDSO for silica particle production. The HMDSO does not only change the flame shape significantly, but also changes the temperature field as it is a fuel itself.

Influence of the air-flow rate

Figure 2 shows particle producing flames at a molar C/H ratio of 0.09 for various air-flow rates at constant HMDSO-nitrogen and hydrogen flow rates of 10 and 24.3 L/min, respectively. Increasing the air-flow rate from 69 to 171 L/min reduces the flame height by 15 cm. Immediately above the burner, the flame is transparent and bluish as combustion of hydrogen takes place first. Above that zone, the flame is white-yellow as combustion of the hydrocarbon component of HMDSO takes place accompanied by silica formation and simultaneous carbon formation, as well as carbon oxidation. As the air-flow rate increases, the gas velocity at the burner exit increases from 5 to 13 m/s resulting in Re_D numbers from 6,000 to 14,000, respectively. In that way the supply of oxygen increases and the mixing of fuel and oxidant intensifies; therefore, the combustion of fuel and precursor is accelerated (Glassman, 1996) and enhanced turbulence causes a diffuse brushy flame (Figure 2d). In addition, the onset of visible particle formation (lower end of the yellowish flame) moves closer to the burner.

Figure 3 shows the specific surface area of the product powder as a function of air-flow rate for hydrogen flow rates of 12.2 and 36.5 L/min at a powder production rate of 300 g/h corresponding to molar C/H ratios of 0.14 and 0.07, respectively. The specific surface area of the product powder increases from 108 to 158 m^2/g (or the average primary particle diameter is reduced from 25 to 17 nm), and the flame height decreases from 55 to 35 cm, when increasing the air-flow rate from 69 to 154 L/min at a hydrogen flow rate of 12.2 L/min (triangles). At the higher hydrogen flow rate (36.5 L/min, circles in Figure 3), increasing the air flow from 86 to 171 L/min increases the specific surface area from 89 to 124 m^2/g (corresponding to average primary particle diameters of 31 and 22 nm, respectively) and the flame height is reduced from 50 to 40 cm. These data are in agreement with Briesen et al. (1998b) who observed a decrease of the flame from 7.5 to 5 cm and a steady increase of the specific surface area from 170 to 230 m^2/g by increasing the total oxidant flow from 2.5 to 5.5 L/min of an HMDSO-methane-air diffusion flame.

Increasing the air-flow rate leads to two competing processes. On the one hand, higher air flow increases the oxidant supply to the reaction zone and reduces the flame height as the fuel is consumed faster. This leads to a higher flame temperature resulting in faster growth and higher sintering

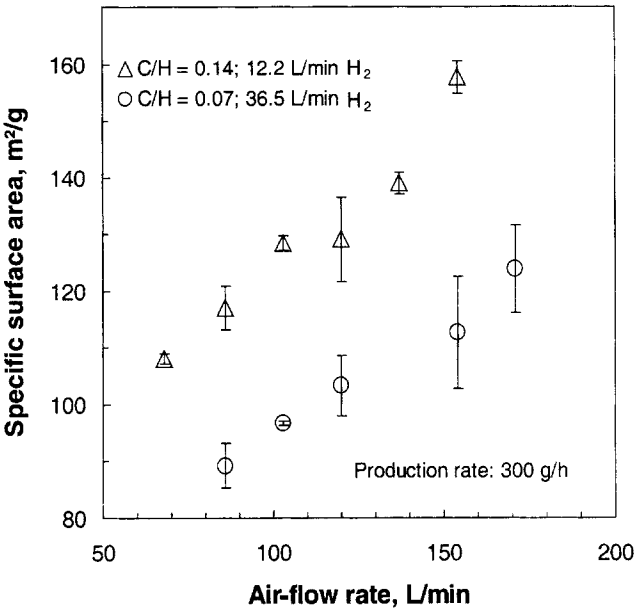

Figure 3. Specific surface area as a function of the air-flow rate at hydrogen flow rate of 12.2 L/min (triangles) and 36.5 L/min (circles) at powder production rates of 300 g/h.

rates and, therefore, to a decrease in the specific surface area. On the other hand, the increase of the air-flow rate also increases the amount of inert gas (nitrogen from the air) delivered to the flame, which would otherwise increase the flame height and lower the flame temperature. At the same time, turbulence of the jet increases when the air-flow rate is increased, accelerating combustion that shortens the flame. The lower flame temperature decreases the particle sintering rate, and the shorter flame and faster gas velocity lead to shorter residence times in the hot flame region. Both effects reduce product particle size; thus, larger specific surface area particles are formed. Clearly, the intensity of the turbulence here dominates with increasing air-flow rate that increases the specific surface area (Figure 3).

Representative TEM-pictures of powders made at production rates of 300 g/h using 12.2 L/min hydrogen are presented for 69 L/min air (Figure 4a) and for 154 L/min air (Figure 4b). The powders are aggregated and partly sintered, but the average primary particle sizes obtained by counting (22 and 14 nm, respectively) agree well to the calculated values by nitrogen adsorption (BET; 25 and 17 nm, respectively). The difference between the data indicate aggregation which is consistent with Figure 4.

Now, increasing the supplied hydrogen flow rate from 12.2 to 36.5 L/min leads to smaller specific surface areas at the higher hydrogen flow rate. The slope of increasing specific surface area with air-flow rate slightly decreases (Figure 3). The cooling effect of the air-flow rate is less significant at higher hydrogen flow rates as additional air accelerates oxygen-hydrogen combustion and subsequently increases the flame temperature. This is in agreement with Pratsinis et al. (1996), where an increase of the fuel flow rate decreased the

specific surface area of the product TiO_2 particles as higher flame temperatures were achieved.

The effect of air entrainment in the flame was investigated by carrying out experiments in the absence and in the presence of the chimney surrounding the flame. Withdrawing the chimney, extra oxygen is drawn into the flame by entrained secondary air leading to faster fuel consumption and, therefore, to higher flame temperature. As a result, the sintering rate increases leading to larger particles and, therefore, to a decrease of the specific surface area (by 14–17%) for air-flow rates less than 120 L/min. At high excess air-flow rates (air number $\lambda = 1.7–1.9$), no differences in the specific surface area are observed ($\pm 3\%$). This may indicate that at high production rates that are typically encountered in industry, air entrainment will not affect the characteristics of the product powder.

Influence of the hydrogen flow rate

Figure 5 shows axial flame temperature profiles for three hydrogen flow rates at constant C/O ratio of 0.12 (production rate 300 g/h SiO_2 and air-flow rate 120 L/min). The temperature increases rapidly with increasing distance from the burner, then almost reaches a plateau at maximum flame temperature, and then decreases slowly. Increasing the hydrogen flow from 12.2 (triangles) to 36.5 L/min (circles) increases the maximum flame temperature from 1,350 to 1,440 K. This trend is in agreement with detailed investigations in hydrogen-oxygen diffusion flames by Choi et al. (1999). Figure 6 shows the influence of the hydrogen flow rate on the specific surface area of the product powder for production rates of 300 g/h and an air-flow rate of 120 L/min (C/O = 0.12). Increasing the hydrogen flow rate from 12.2 to 42.5 L/min decreases the specific surface area from 129 to 96 m^2/g. Increasing the hydrogen flow rate results in higher flame temperature (Figure 5) that increases the sintering rate of the particles and, therefore, results in larger particles and smaller specific surface areas. Performing full adsorption and desorption isotherms shows that particles are nonporous, while the corresponding t-plot indicates very small slit-shaped pores (Lippens and de Boer, 1965), which are attributed to the necks between the particles in the aggregates.

Influence of the production rate

The silica production rate was set by controlling the HMDSO flask temperature for carrier gas-flow rate of 10 L/min. Figure 7 shows the specific surface area of powders made at three production rates as a function of the air-flow rate at hydrogen flow rate of 12.2 L/min. The molar C/H ratios are 0.14 (triangles), 0.11 (squares), and 0.08 (diamonds), respectively. Decreasing the production rate from 300 g/h (triangles) to 200 g/h (squares) and 125 g/h (diamonds) increases the specific surface area of the product powder from 139 to 186 and 249 m^2/g, respectively, for an air-flow rate of 137 L/min. Correspondingly, the primary particle diameter decreases from 20 to 15 and 11 nm. As the HMDSO concentration decreases with decreasing production rate, the adiabatic flame temperature decreases as less fuel (hydrogen and HMDSO) is supplied (the total thermal input decreases from

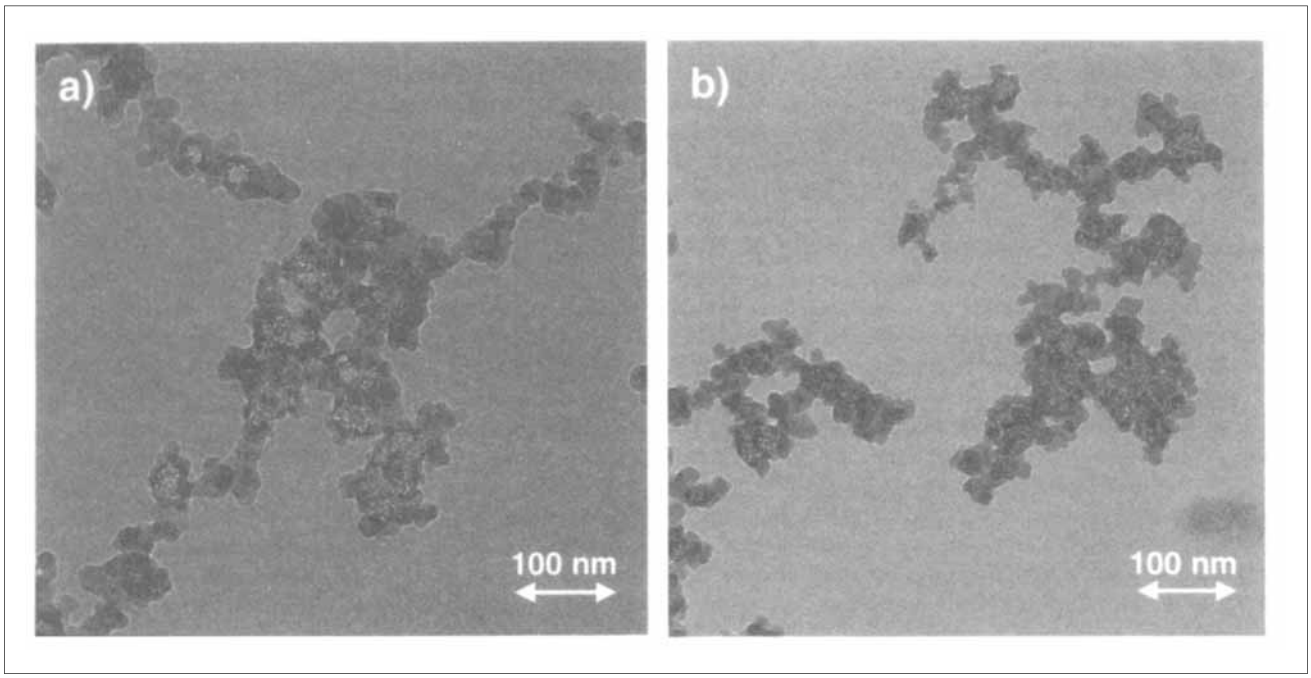

Figure 4. Transmission electron micrographs of silica-carbon powders at production rates of 300 g/h, using 12.2 L/min hydrogen and 69 L/min air (a) and 154 L/min air (b), respectively.

The corresponding average primary particle diameters calculated from nitrogen adsorption (BET) are 25 nm (a) and 17 nm (b), while 22 nm (a) and 14 nm (b) were obtained by TEM counting, respectively.

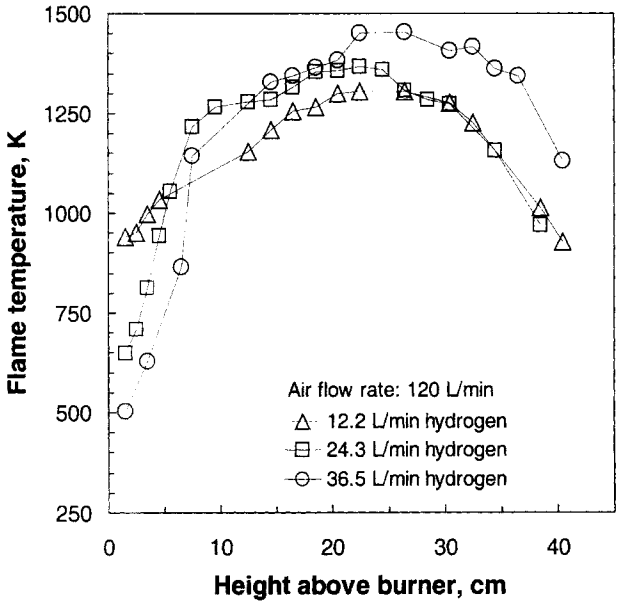

Figure 5. Axial temperature profile along the center line of the particle laden flame for production rates of 300 g/h for hydrogen flow rates of 12.2 (triangles), 24.3 (squares), and 36.5 L/min (circles).

The temperatures are corrected by radiation loss according to Collins and Williams (1959).

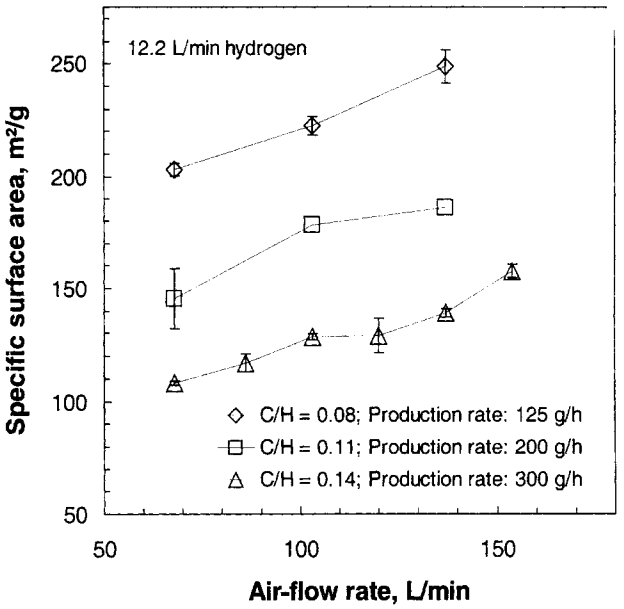

Figure 7. Specific surface area as a function of the air-flow rate for production rates of 125 g/h (diamonds), 200 g/h (squares), and 300 g/h (triangles).

The hydrogen flow rate was 12.2 L/min.

5.9 to 3.6 kW reducing the production rate from 300 to 125 g/h). As a result of the lower flame temperature, the sintering rate is decreased which leads to higher specific surface areas. The decrease of particle concentration leads to subsequently fewer particle collisions and less growth as less precursor is delivered into the flame. Reducing the powder production rate from 300 to 125 g/h by reducing the HMDSO concentration decreases the visible flame height from 50 to 30 cm for a constant air-flow rate of 103 L/min.

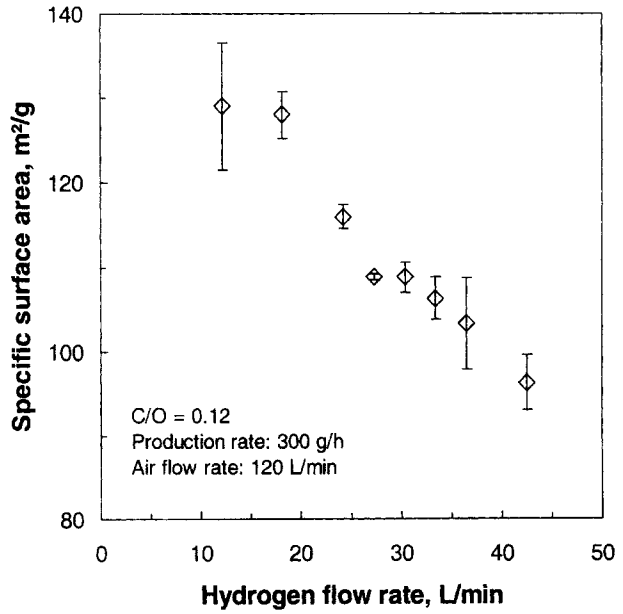

Figure 6. Specific surface area as a function of the hydrogen flow rate with 120 L/min air at production rate of 300 g/h.

Lower production rates lead to significantly larger specific surface areas in agreement with Kammler and Pratsinis (1999). In that earlier study with significantly lower burner exit velocities (0.3 m/s), increasing the powder production rate from 22 to 130 g/h decreased the specific surface area from 175 to 19 m^2/g, as oxygen leads to much higher flame temperatures resulting in faster sintering and significantly smaller specific surface areas compared to the present powders (Zhu and Pratsinis, 1997). Increasing the HMDSO delivery rate increases the fuel input into the flame, resulting in higher flame temperatures and flame heights and, therefore, longer residence times of the particles at high temperatures. Hence, particle growth takes place faster and bigger particles are formed as a result of the enhanced sintering rates.

Figure 8 shows the specific surface area of the product powder as a function of production rate at hydrogen and air-flow rates of 12.2 and 103 L/min, respectively. Continuous operation of the turbulent hydrogen-air flame is demonstrated by operating the unit for 5 h at production rates of 700 g/h. As the production rate is increased from 125 to 700 g/h, corresponding to an increase of the SiO_2 mass concentration from 17 to 93 g/m^3, the specific surface area decreased from 222 to 75 m^2/g. The higher the HMDSO concentration in the reactant stream, the higher is the adiabatic flame temperature leading to enhanced sintering that results in lower specific surface areas. Increasing the production rate

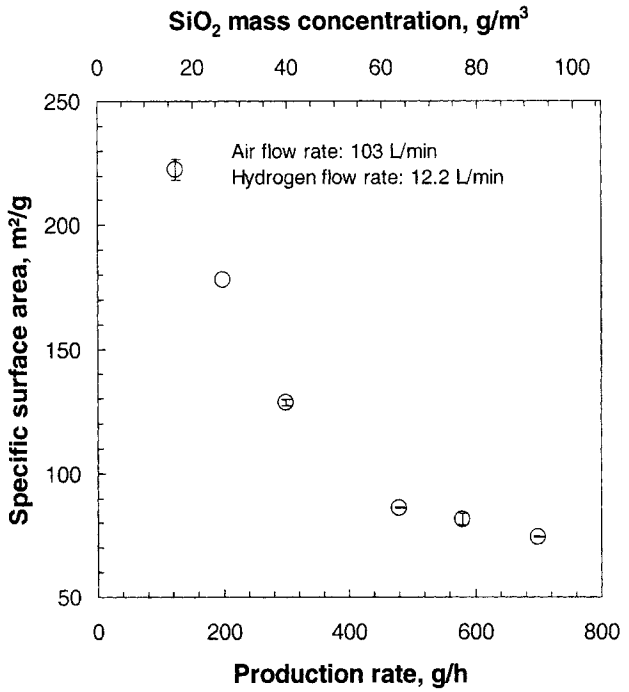

Figure 8. Specific surface area as a function of the production rate and SiO_2 mass concentration at 10 L/min nitrogen (through the HMDSO), 12.2 L/min hydrogen, and 103 L/min air.

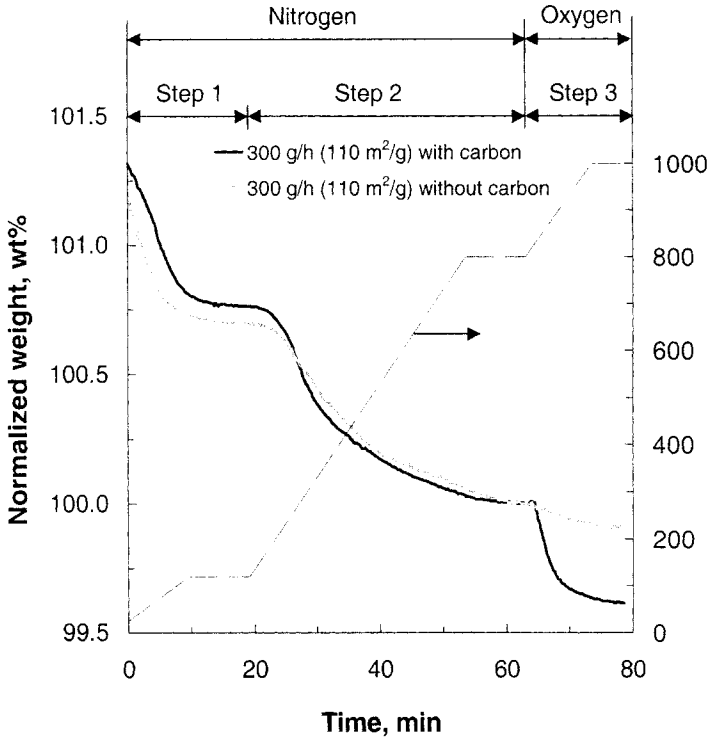

Figure 9. Sample weight normalized to the sample weight after the second step [removal of physically and chemically bound water (and volatiles)] as a function of time and temperature.

It was determined by thermogravimetry for pure silica (thin line) and carbon containing (thick line) powders of specific surface area of 110 m^2/g.

from 125 to 700 g/h by increasing the HMDSO delivery rate (by increasing the HMDSO flask temperature) increases the total fuel input into the flame (3.6 kW to 11.0 kW), and the flame height is increased from 30 to 70 cm. However, this results in longer residence times of the particles at high temperatures; therefore, particle growth takes place faster and, as a result of the enhanced sintering rates, bigger particles are formed. The increase of HMDSO concentration also increases the silica particle concentration leading to subsequently more particle collisions, and, therefore, enhanced growth which increases the particle diameter as well. These results are in agreement with studies at lower powder production rates, where an increase in the precursor concentration decreased the specific surface area of the powders (Briesen et al., 1998a,b; Kammler and Pratsinis, 1999, 2000) but do not agree with Ulrich and Riehl (1982) and Fotou et al. (1995), who did not observe a significant influence of the particle concentration. This is attributed to the fact that the energy of combustion of HMDSO is larger than that of $SiCl_4$ oxidation (Briesen et al., 1998b; Kammler and Pratsinis, 1999).

Powder composition

Using hydrogen as fuel has the advantage over hydrocarbon fuels (such as methane) since it does not contain carbon; therefore, the precursor itself is the only source for carbon formation. Typically, in diffusion flames carbon inception occurs around 1,400 K and depends on hydrogen atom diffusion (Glassman, 1988). As shown in Figure 5, the maximum flame temperatures are close to or even above this value, as particle coating on the thermocouple tip lowers the measured temperature (Chung and Katz, 1985).

All powders are gray at production rates of 300 g/h using 12.2 L/min hydrogen (Figure 3: triangles) indicating that the oxidation of HMDSO is incomplete, even at excess oxygen. In contrast, powders produced at 300 g/h with 36.5 L/min hydrogen (Figure 3: circles) are white. White powders are produced as well at lower production rates (Figure 7: diamonds and squares and Figure 8). In Figure 6 the color of the powders changes from gray to white with increasing hydrogen flow.

A typical thermogravimetric analysis plot is shown in Figure 9, in which white powder (thin solid line) and carbon containing gray powder (thick solid line) of the same specific surface area (110 m^2/g) are compared. The sample weight is monitored with time during the temperature program, which is indicated by the dotted line, consisting of isothermal and dynamic segments.

Increasing the temperature from 25 to 120°C in nitrogen atmosphere removes the physically adsorbed water from the silica powder surface (Hockey, 1965; Iler, 1979) and is not crucial for the powder characterization as it depends, for example, on the actual humidity of the surrounding air and sample preparation. The removal of physically bound water is referred here as the first step. The second step (from 120 to 800°C in nitrogen) represents the loss in weight from the reduction of silanol groups on the powder surface, the so-called chemically bound water (Iler, 1979). Of course, there is also

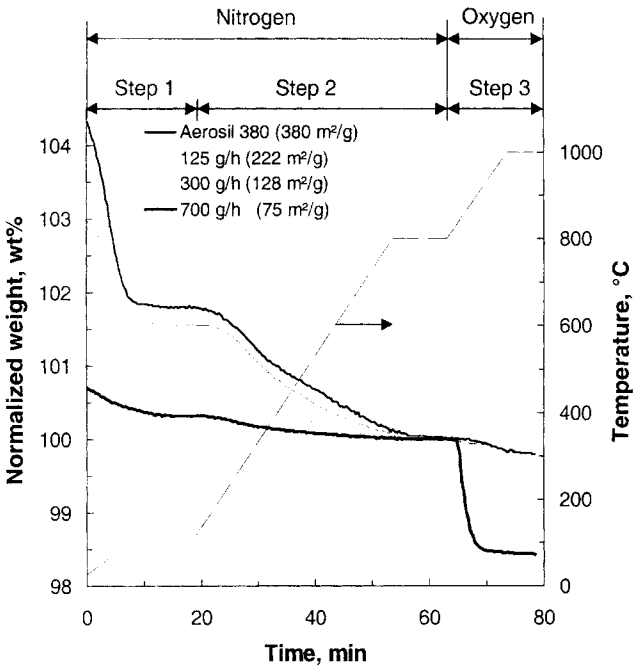

Figure 10. Sample weight normalized to the sample weight after the second step [removal of physically and chemically bound water (and volatiles)] as a function of time and temperature.

It was determined by thermogravimetry for powders made at production rates of 125, 300 and 700 g/h, corresponding to Figures 8 and 11, and commercial available fumed silica (Aerosil 380).

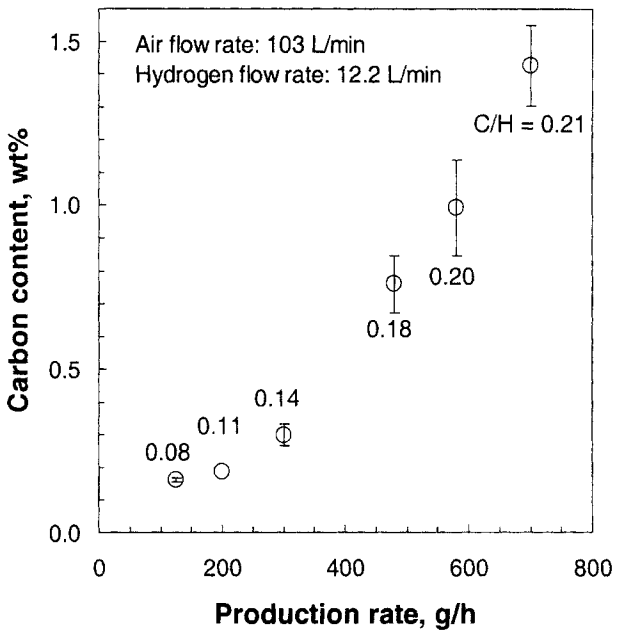

Figure 11. Carbon content of product powders as a function of production rate.

Also shown is the corresponding C/H ratio. The gas-flow rates are 10 L/min nitrogen (through the HMDSO), 12.2 L/min hydrogen, and 103 L/min air.

the possibility that easily volatizable compounds are removed with the chemically bound water from the powder surface by the temperature treatment, but the TGA effluent gas analysis indicated that this amount is less than 5%. It was shown with nitrogen adsorption (BET-method) that the specific surface area of the powders remained constant up to 800°C, by analyzing powders before and directly after the heating period. This indicates that the surface area of the powders was not significantly modified, such as by evaporation of volatiles or volatile carbon, which would cause an increase of specific surface area as observed by Spicer et al. (1998) for carbon black-fumed silica powders.

The weight loss from 800 to 1,000°C in oxygen (third step), however, represents the carbon content (black carbon) of the powder that is verified by analyzing the CO_2 concentration of the off-gases from the thermobalance with a CO_2 detector assuming stoichiometric oxidation. For gray powder, a significant decrease in the normalized weight is detected in the third step resulting from carbon oxidation. A fraction of this loss in weight of the third step results from the residual OH-groups per nm^2 at 800°C (0.9 OH-groups per nm^2), which is reduced to 0.4 OH-groups per nm^2 at 1,000°C (Curthoys et al., 1974). This fraction is negligible for carbon containing powders, but explains the small weight loss of the perfectly white powders (Figures 9 and 10).

Figure 10 shows the normalized sample weight during TGA for powders produced at 125, 300 and 700 g/h (from Figure 8) and Aerosil 380 (Degussa-Huels AG), respectively. As discussed in Figure 9, physically adsorbed water (first step), chemically bound water and volatile compounds (second step), and the carbon content (third step) can be determined. Here, it can be seen clearly that both the physically (first step) and chemically (second step) bound water depend strongly on the specific surface area of the powders as the total amount of silanol groups increases for increasing specific surface area and constant OH-group density (OH-groups per nm^2 powder surface). This explains the larger loss in weight in the first and second step for Aerosil 380 and the powder made at production rates of 125 g/h (specific surface areas of 380 and 222 m^2/g, respectively) compared to the powders produced at 300 and 700 g/h with specific surface areas of 128 and 75 m^2/g, respectively. The weight loss from 800 to 1,000°C in oxygen (third step) is very small for Aerosil 380 and the perfectly white powder produced at production rates of 125 g/h (further OH-removal), but is significant for gray powders and increases with their increasing carbon content. Comparison of the TGA plot of Aerosil 380 and the white powder (thin solid line; 125 g/h) shows similar behavior in all three steps during TGA, indicating similar powder composition.

Figure 11 shows the carbon content (third step) as a function of the powder production rate. The powders were made at hydrogen and air-flow rates of 12.2 and 103 L/min, respectively, corresponding to Figures 8 and 10. Increasing the production rate from 125 to 700 g/h increases progressively the amount of carbon in the powder from 0.15 to 1.4 wt. % (Figure 11). The small loss in weight for the first two points (white powders) in this figure is attributed to OH-removal as discussed above. As the amount of supplied air was held constant, the ratio of fuel to oxidant increases with an increasing production rate; thus, under stoichiometric amounts (air number $\lambda = 0.7$) are reached for production rates of 700 g/h,

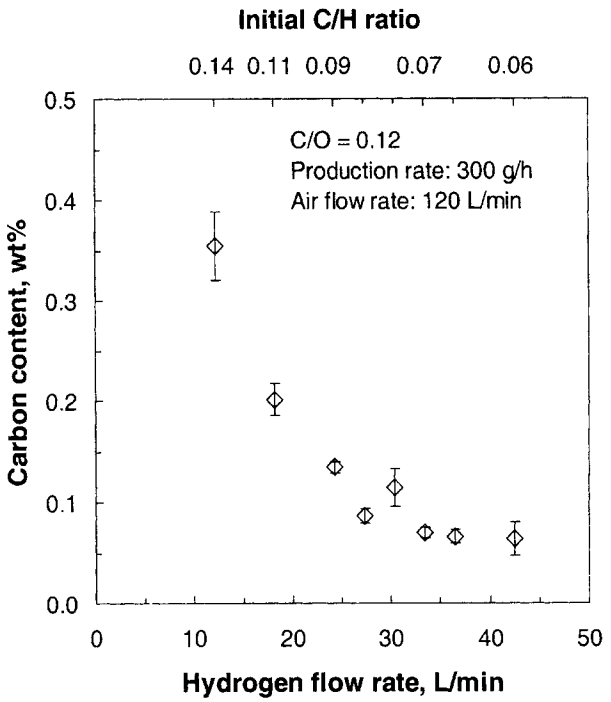

Figure 12. Carbon content of product powders determined with thermogravimetric analysis (third step) as a a function of the hydrogen flow rate and molar C/H ratio at C/O ratio of 0.12.

These data correlate to the data of Figure 6.

while there is an excess of oxygen for production rates of 125, 200, and 300 g/h (the corresponding air numbers are 2.2, 1.8, and 1.2). Generally, in laminar hydrocarbon diffusion flames the soot fraction increases with temperature (Schug et al., 1980; Glassman and Yaccarino, 1981). This is in agreement with Figure 11 since, as the hydrocarbon containing HMDSO concentration increases, more carbon is formed. The decrease of the specific surface area (Figure 8) indicates higher temperatures which increase particle growth and sintering. The molar C/H ratio increases with increasing HMDSO flow rate. It appears that white powders are formed below C/H ~0.12, while the carbon content increases above this ratio.

Figure 12 shows the carbon content (third step) of powders (production rate 300 g/h) at different hydrogen flow rates (corresponding to Figure 6) at constant air-flow rate of 120 L/min. At hydrogen flow rates of 12.2 L/min, the powders contain 0.43 wt. % carbon when overall excess of oxygen is provided (air number $\lambda = 1.4$). The carbon content decreases with increasing hydrogen flow rate and at hydrogen flow rates of more than 18.2 L/min; virtually no carbon remains in the product powder (they are perfectly white). Increasing the hydrogen flow even more the flame becomes fuel rich ($\lambda = 0.8$ for 42.5 L/min hydrogen), but no carbon remains in the product powder. This is attributed to the higher flame temperatures (Figure 5) oxidizing carbon completely and to the increased hydrogen concentration as hydrogen radicals are known to accelerate normal pyrolysis reactions by diffusion into fuel rich zones (Glassman, 1988). Complete carbon oxidation is achieved here when increasing the total fuel input by hydrogen addition in contrast to enhanced carbon formation when the hydrocarbon (HMDSO) increases the fuel input (Figure 11). The perfectly white powders produced, for example, with 36.5 L/min hydrogen, lose very little weight (up to 0.07 wt. %) due to removal of chemically bound water from the powders (in agreement with Figures 9 and 10).

Calculating the molar C/H ratio (upper x-axis in Figure 12), it appears that no carbon remains in the product powder when this ratio exceeds ~ 0.12, the same value as observed in Figure 11. Schug et al. (1980) proposed that the C/H ratio does not determine the sooting height or composition of the fuel mixture as a responsible (general) parameter for the sooting criterion. More generally, investigating different fuel mixtures in air diffusion flames, the maximum sooting height of the mixture is determined by the sooting height of the pure additive. For fuel mixtures of hydrocarbons with hydrogen, asymptotic values of the sooting height (sooting height $\rightarrow \infty$) are achieved when the C/H ratio is decreased to a critical C/H value, below which sooting cannot be observed. This may depend on the choice of the hydrocarbon and may depend also on burner geometry or other parameters, but it seems to describe the ability of a certain system to soot. Therefore, the C/H ratio may be used to describe individual burner systems and guide the production of silica powders of a certain carbon composition. As the sooting height describes the sooting tendency of a system—the smaller the sooting height, the larger the ability to soot—the C/H value for the investigated system can also give a qualitative estimate of the carbon content in the product powder. The critical C/H ratio of ~ 0.12 here is in agreement with the asymptotic value for the sooting height for acetylene-hydrogen mixtures by Schug et al. (1980).

According to EDX analysis, the white powders did not contain carbon. For the carbon silica powders, there was no evidence even in the darkest powders that the particles were film coated. These observations indicate that the carbon and silica particles are separate. As more fuel from HMDSO is supplied into the flame, the associated CH_3^+ concentration increases. Therefore, more carbon enters the system. When HMDSO is pyrolyzed first, the C-Si bonds are split resulting in separate formation of silica and hydrocarbon that will be converted to soot or carbon black, as observed in the product powder by STEM/EDX (Nicholls, 1999). This indicates that the carbon may not grow on the silica particles, but rather carbon and silica particles coagulate resulting in a spotty-coating of the silica aggregates with carbon nanoparticles.

Conclusions

For the first time, a systematic investigation of flame synthesis of nanoparticles at high production rates (up to 700 g/h) was carried out. The effect of process variables on the characteristics of product silica-carbon particles was investigated in a turbulent air-hydrogen diffusion flame reactor. The specific surface area of the product powder was controlled in the range of 75 to 250 m^2/g by reactant stream composition. Increasing the production rate from 125 to 700 g/h decreased the specific surface area from 222 to 75 m^2/g for constant air-flow rate of 103 L/min and increased the carbon content of the powder. Increasing the air-flow rate, however,

increases the specific surface area and does not depend on the overall-stoichiometry of the flame in the investigated range. Decreasing the hydrogen concentration increases the specific surface area and the carbon content of the product powder, as was determined by thermogravimetric analysis (TGA) coupled with mass spectroscopy (MS). The silica aggregates are spotty-coated with carbon implying that carbon and silica particles form separately and coagulate downstream.

Acknowledgments

This article was presented at the Annual AIChE Meeting in Los Angeles, November, 2000. We acknowledge financial support by the Swiss National Science Foundation. We thank Dr. R. J. Geier (BASF, Ludwigshafen, Germany) for help and advice on the buildup of the pilot plant and the safety concept; Dr. C. M. Megaridis and Dr. A. W. Nicholls (both from University Illinois, Chicago) for the TEM/STEM and EDX analysis; and Dr. M. Müller (ETH Zürich) for help with TEM.

Literature Cited

Blume, H., "Analytical Properties of Silica—A Key for Understanding Silica Reinforcement," *Kautsch. Gummi Kunstst.*, **53**, 338 (2000).

Bomal, Y., P. Cochett, B. Dejean, J. Machurat, and I. Gelling, "Influence of Mixing Procedures on the Properties of a Silica Reinforced Agricultural Tire Tread," *Rubber World*, **208**, 33 (1993).

Boublik, T., V. Fried, and E. Hala, *The Vapour Pressures of Pure Substances*, Elsevier, Amsterdam (1984).

Bray, K. N. C., "The Challenge of Turbulent Combustion," *Int. Symp. on Combustion*, Combustion Inst., p. 1 (1998).

Briesen, H., A. Fuhrmann, and S. E. Pratsinis, "Electrically Assisted Aerosol Reactors Using Ring Electrodes," *Nanostructured Powders and Their Industrial Applications*, G. Beaucage, G. Burns, H. Duen-Wu and J. E. Mark, eds., *MRS Symp. Proc.*, **520**, 3 (1998a).

Briesen, H., A. Fuhrmann, and S. E. Pratsinis, "The Effect of Precursor in Flame Synthesis of SiO_2," *Chem. Eng. Sci.*, **53**, 4105 (1998b).

Byers, J. T., and A. A. McNeish, "Current Advances in Tire Compounding Technology for Low Rolling Resistance," Carbon Black World Conf., San Antonio, TX (Mar. 19–21, 1997).

Choi, M., J. Cho, J. Lee, and H. W. Kim, "Measurements of Silica Aggregate Particle Growth Using Light Scattering and Thermophoretic Sampling in a Coflow Diffusion Flame," *J. Nanoparticle Res.*, **1**, 169 (1999).

Chung, S.-L., and J. L. Katz, "The Counterflow Flame Burner: A New Tool for the Study of Nucleation of Refractory Compounds," *Combust. Flame*, **61**, 271 (1985).

Collis, D. C., and M. J. Williams, "Two Dimensional Convection from Heated Wires at Low Reynolds Numbers," *J. Fluid Mech.*, **6**, 357 (1959).

Curthoys, G., V. Y. Davydov, A. V. Kiselev, S. A. Kiselev, and B. V. Kuznetsov, "Hydrogen Bonding in Adsorption on Silica," *J. Colloid Interface Sci.*, **48**, 58 (1974).

Donnet, J., R. C. Bansal, and M.-J. Wang, *Carbon Black*, Marcel Decker, New York (1993).

Fotou, G. P., S. J. Scott, and S. E. Pratsinis, "The Role of Ferrocene in Flame Synthesis of Silica," *Combust. Flame*, **101**, 529 (1995).

Francis, R. A., K. Mahmud, J. A. Belmont, and M.-J. Wang, Patent No. WO9637547 (1996).

Geier, R. J., "Coal Pyrolysis at High Solids Loadings in a Download Tube Reactor," *Fortschritt-Bericht*, VDI Verlag, Reihe 3, Verfahrenstechnik, Nr. 566 (1998).

Glassman, I., and P. Yaccarino, "The Temperature Effect in Sooting Diffusion Flames," *Int. Symp. on Combustion*, Combustion Inst., p. 1175 (1981).

Glassman, I., "Soot Formation in Combustion Processes," *Int. Symp. on Combustion*, Combustion Inst., p. 295 (1988).

Glassman, I., *Combustion*, Academic Press, San Diego (1996).

Hockey, J. A., "The Surface Properties of Silica Powders," *Chem. Ind.*, **57** (1965).

Iler, R. K., *The Chemistry of Silica*, Wiley, New York (1979).

Kammler, H. K., and S. E. Pratsinis, "Scaling-Up the Production of Nanosized SiO_2-Particles in a Double Diffusion Flame Aerosol Reactor," *J. Nanoparticle Res.*, **1**, 467 (1999).

Kammler, H. K., and S. E. Pratsinis, "Electrically-Assisted Flame Aerosol Synthesis of Fumed Silica at High Production Rates," *Chem. Eng. Process.*, **39**, 219 (2000).

Kloepfer, H., German Patent No. DE 762 723 (1942).

Koc, R., and S. V. Cattamanchi, "Synthesis of Beta Silicon Carbide Powders Using Carbon Coated Fumed Silica," *J. Mater. Sci.*, **33**, 2537 (1998).

Lee, D., P. C. Stevens, and A. J. Hunt, "Thermal Characterization of Carbon-Opacified Silica Aerogels," *J. Non. Cryst. Solids*, **186**, 285 (1995).

Lippens, B. C., and J. H. de Boer, "Studies on Pore Systems in Catalysts: V. The *t*-Method," *J. Catal.*, **4**, 319 (1965).

Nicholls, A., personal communication (1999).

Padula, S., "Tire Fuel Economy Labeling—An Update," Tire Industry Conference, Hilton Head, SC (Mar. 9–10, 1995).

Pratsinis, S. E., W. Zhu, and S. Vemury, "The Role of Gas Mixing in Flame Synthesis of Titania Powders," *Powder Technol.*, **86**, 87 (1996).

Pratsinis, S. E., "Flame Aerosol Synthesis of Ceramic Powders," *Prog. Energy Combust. Sci.*, **24**, 197 (1998).

Schug, K. P., Y. Manheimer-Timnat, P. Yaccarimo, and I. Glassman, "Sooting Behavior of Gaseous Hydrocarbon Diffusion Flames and the Influence of Additives," *Combust. Sci. Technol.*, **22**, 235 (1980).

Sniegowski, J. J., and M. P. de Boer, "IC-Compatible Polysilicon Surface Micromachining," *Annu. Rev. Mater. Sci.*, **30**, 299 (2000).

Spicer, P. T., C. Artelt, S. Sanders, and S. E. Pratsinis, "Flame Synthesis of Composite Carbon Black-Fumed Silica Nanostructured Particles," *J. Aerosol. Sci.*, **29**, 647 (1988).

Tacke, M. M., T. C. Cheng, E. P. Hassel, and J. Janicka, "Study of Swirling Recirculating Hydrogen Diffusion Flame Using UV Raman Spectroscopy," *Int. Symp. on Combustion*, Combustion Inst., p. 169 (1996).

Turns, S. R., *An Introduction to Combustion: Concepts and Applications*, McGraw-Hill, New York (1996).

Ulrich, G. D., and J. W. Riehl, "Aggregation and Growth of Submicron Oxide Particles in Flames," *J. Colloid Interface Sci.*, **87**, 257 (1982).

Ulrich, G. D., "Flame Synthesis of Fine Particles," *Chem. Eng. News*, **62**, 22 (1984).

Wang, M.-J., K. Mahmud, L. J. Murphy, and W. J. Patterson, "Carbon-Silica Dual Phase Filler, A New Generation Reinforcing Agent for Rubber," *Kautsch. Gummi Kunstst.*, **51**, 338 (1998).

Zhu, W., and S. E. Pratsinis, "Synthesis of SiO_2 and SnO_2 Particles in Diffusion Flame Reactors," *AIChE J.*, **43**, 2657 (1997).

Manuscript received May 16, 2000, and revision received Dec. 15, 2000.